IOP Publishing Journal of Physics: Condensed Matter
J. Phys.: Condens. Matter **27** (2015) 335504 (6pp) doi:10.1088/0953-8984/27/33/335504

Calculation of the specific heat of optimally K-doped $BaFe_2As_2$

Hyungju Oh, Sinisa Coh and Marvin L Cohen

Department of Physics, University of California at Berkeley and Materials Sciences Division, Lawrence Berkeley National Laboratory, Berkeley, CA 94720, USA

E-mail: xtom97@civet.berkeley.edu

Received 15 May 2015, revised 7 July 2015
Accepted for publication 8 July 2015
Published 4 August 2015

Abstract

The calculated specific heat of optimally K-doped $BaFe_2As_2$ in density functional theory is about five times smaller than that found in the experiment. We report that by adjusting the potential on the iron atom to be slightly more repulsive for electrons improves the calculated heat capacity as well as the electronic band structure of $Ba_{0.6}K_{0.4}Fe_2As_2$. In addition, structural and magnetic properties are moved in the direction of experimental values. Applying the same correction to the antiferromagnetic state, we find that the electron–phonon coupling is strongly enhanced.

Keywords: optimally K-doped $BaFe_2As_2$, specific heat, semi-empirical density functional theory

(Some figures may appear in colour only in the online journal)

1. Introduction

The discovery [1] of superconductivity in $LaFeAsO_{1-x}F_x$ with a transition temperature of 26 K in 2008 triggered unprecedented interest and further research in iron-based superconductors. So far, superconductivity was found in four main families of iron-based compounds: 1111, 122, 111, and 11 [2, 3]. These iron-based materials have two phases in the normal state: one is a paramagnetic metal and the other is an antiferromagnetic metal. Superconductivity emerges in both the paramagnetic and antiferromagnetic metal phases via application of hydrostatic pressure or carrier doping of the parent materials. Hence, it is expected that understanding the electronic and magnetic structures of the metallic normal states of these systems is a needed ingredient for unraveling the origin of the superconductivity of iron-based materials.

Many experimental and theoretical studies have been made on the normal states of iron-based superconductors, and a consensus [4, 5] has been reached in these systems that the Coulomb interaction among the electrons is not strong enough to induce a Mott insulating phase. However, the Coulomb interaction plays an important role in determining the electric and magnetic properties. In the early stages of this research, theoretical insight into the properties of these materials was gained by calculations based on density functional theory (DFT) within the local density approximation (LDA) or generalized gradient approximation (GGA). However, LDA and GGA have some limitations in describing the normal states of iron-based superconductors. In a paramagnetic phase, the measured mass of low-energy quasiparticles [6] is 2–3 times larger than that calculated within LDA or GGA. In addition, the measured magnitude of the ordered moment in an antiferromagnetic phase [7, 8] is 2–3 times smaller than that obtained with LDA or GGA. Furthermore, LDA and GGA studies related to the specific heat of these materials are not consistent with the experimental data. The theoretical Sommerfeld coefficient [9–11] of optimally K-doped $BaFe_2As_2$ is about five times smaller than that found in the experimental data [12–16].

There have been many attempts to describe electronic correlations in these materials by combining LDA or GGA calculations with a dynamical mean-field theory (DMFT), quasiparticle self-consistent GW (QSGW), or the Gutzwiller method [17–20]. Using these methods, many of the electric and magnetic properties of correlated iron-based superconductors can be reproduced. For example, effective masses and Fermi surfaces (FSs) across all families of iron compounds are well described in the framework of DFT + DMFT [17] and QSGW [18], as well as ordered moments and the fluctuations of local moments within DFT + DMFT [17, 19]. However, a calculation of the electron–phonon coupling coefficient

(which is needed for heat capacity and superconductivity estimates) within these approaches is non-trivial. Therefore, we use a simpler method to calculate electronic and magnetic properties of these materials.

In this work we study the heat capacity of $Ba_{0.6}K_{0.4}Fe_2As_2$ superconductor ($T_c = 38$ K) [21] within a semi-empirically modified GGA potential, following studies [22] of an FeSe monolayer. We show that one can choose a small repulsive potential located on the iron atoms (+A term) so that the calculated specific heat coefficient is increased from $\gamma_n = 12$ mJ mol^{-1} K^{-2} in GGA to $\gamma_n = 38$ mJ mol^{-1} K^{-2} in GGA + A, much closer to recent experimental findings ($\gamma_n = 40 - 50$ mJ mol^{-1} K^{-2}) [12–15]. The increase in γ_n relative to GGA comes mostly from the increased density of states (DOS) at the Fermi level and to a smaller extent from an enhanced electron–phonon coupling. Since $Ba_{0.6}K_{0.4}Fe_2As_2$ is near a magnetic phase transition, we also computed the heat capacity in the striped antiferromagnetic ground state, present in the parent compound. Just as in the nonmagnetic calculation, we again find an increased γ_n (from 6 to 12 mJ mol^{-1} K^{-2}) when +A term is added. However, unlike in the nonmagnetic calculation, the increased γ_n originates mostly from increase in the electron–phonon coefficient λ.

The focus of this work is on the heat capacity and the electronic structure of $Ba_{0.6}K_{0.4}Fe_2As_2$. The microscopic origin for the success of the semi-empirical approach (+A) is left for future studies. We only note here that the success of this approach is not limited to $Ba_{0.6}K_{0.4}Fe_2As_2$, but that it also improves [22] calculated properties for a range of transition-metal compounds ($KCuF_3$, $LaNiO_3$, $(La,Sr)_2CuO_4$, $SrTiO_3$, and FeSe monolayer), and that this approach is similar in spirit to earlier empirical methods [23, 24]. For all the compounds, the +A term modifies the d levels of transition metals reducing the electron density near the transition metal sites. This implies that LDA/GGA might overestimate d-level filling in a transition-metal compounds.

2. Methods

Our calculations are based on norm-conserving pseudopotentials and the Perdew–Burke–Ernzerhof [25] functional as implemented in the SIESTA code [26]. Electronic wavefunctions are expanded with pseudoatomic orbitals (double-ζ polarization). We treat the potassium doping within the virtual crystal approximation.

Following [22] we modify the GGA potential $V_{GGA}(\mathbf{r})$ by adding a repulsive potential on each iron atom in the calculation during the self-consistency loop,

$$V_{GGA}(\mathbf{r}) + A \sum_i f(|\mathbf{r} - \mathbf{r}_i|). \quad (1)$$

Here $f(r)$ is a positive dimensionless function peaked at the nucleus of the iron atoms ($\mathbf{r}_i$) and the extent of $f(r)$ is comparable with the size of d orbitals in the iron atoms. We discuss the choice of A and $f(r)$ in section 2.1.

The GGA + A approach can be understood as a variant of the constrained DFT (CDFT) formalism [27]. The CDFT approach adds a general constraint to the density,

$$\sum_\sigma \int w_c^\sigma(\mathbf{r})\rho^\sigma(\mathbf{r})\, d\mathbf{r} = N_c, \quad (2)$$

where $w_c(\mathbf{r})$ acts as a weight function that defines the constrained property. The Kohn–Sham total energy is minimized under the constraint from equation (2), by making the following functional stationary,

$$W[\rho, V_c] = E[\rho] + V_c\left(\sum_\sigma \int w_c^\sigma(\mathbf{r})\rho^\sigma(\mathbf{r})d\mathbf{r} - N_c\right). \quad (3)$$

Here V_c is a Lagrange multiplier corresponding to the constraint. Therefore, in the effective Hamiltonian of the CDFT formalism, there is an additional potential $V_c w_c^\sigma(\mathbf{r})$ coming from the constraint. Since the GGA + A potential (equation (1)) has the same form as the constraint potential in the CDFT approach, GGA + A method has the same effect as constraining the number of electrons around the iron atom.

2.1. Choice of A f(r) term

Now we discuss our choice of the correction term $A\ f(r)$ appearing in equation (1).

Following previous work on the FeSe monolayer [22] we first choose $f(r) = e^{-1.0r^2}$ in atomic units (Bohr radius) with the extend comparable with the size of the iron atom d-orbital. Second, we tune A from 0 up to A_c until one of the properties of $Ba_{0.6}K_{0.4}Fe_2As_2$ agrees better with the experimental data. We choose to tune the occupied bandwidth of the M-point electron pocket since it is severely overestimated in GGA (it is 130 meV in GGA while ∼0–10 meV in the experiment [28, 29]). We find that using $A_c = 1.3$ Ry has the desired effect of tuning the M-point bandwidth to about 4 meV.

Just as in [22] we find that the choice of $f(r)$ is not very important for physical properties as long as it is localized on the iron atom and A is tuned for each choice of $f(r)$. For example, using $Af(r) = 2.2e^{-1.7r^2}$ or $Af(r) = 5.5e^{-3.5r^2}$ results in nearly indistinguishable band structure of $Ba_{0.6}K_{0.4}Fe_2As_2$.

Using $A = A_c$ improves not only the occupied bandwidth of the M-point electron pocket but other properties of $Ba_{0.6}K_{0.4}Fe_2As_2$ as well. For example, structural parameters relevant for superconductivity (arsenic height and iron-arsenic-iron angle) [30–33] are both moved in the direction towards experimental value. However, numerical values of these structural parameters match experimental values for A in between 0 and A_c and are thus overcorrected at $A = A_c$. For example, going from GGA to GGA + A the arsenic height is increased from 1.30 Å to 1.44 Å while the iron-arsenic-iron angle is decreased from 112.5° to 105.9°. Another improvement is that the antiferromagnetic ground state is suppressed in GGA + A. See table 1 for more details. We confirmed that the modifications of structural and magnetic properties are insensitive to the choice of $f(r)$.

Finally, using $A = A_c$ the calculated heat capacity of $Ba_{0.6}K_{0.4}Fe_2As_2$ is more than three times larger as compared to the GGA value, and in good agreement with the experimental value. We discuss heat capacity in more detail in section 4.

Table 1. A comparison of the arsenic height, iron-arsenic-iron angle, lattice constants (a and c), magnetic moment (μ_{Fe}) on iron atom, and the energy difference (ΔE) per one iron atom between antiferromagnetic stripe and nonmagnetic ground state in GGA, GGA + A, and from experiment [21] in $Ba_{0.6}K_{0.4}Fe_2As_2$.

	As height (Å)	Fe–As–Fe (°)	a (Å)	c (Å)	μ_{Fe} (μ_B)	ΔE (eV)
GGA + A	1.44	105.9	3.82	13.89	2.26	–0.19
GGA	1.30	112.5	3.89	13.26	2.91	–0.33
Experiment	1.37	109.9	3.91	13.21		

3. Electronic structure

Now we discuss the electronic structure of $Ba_{0.6}K_{0.4}Fe_2As_2$ in GGA and GGA + A. In all of our calculations we perform a full structural relaxation for both forces on atoms and stresses on the cell. We used double zeta polarized basis and a charge density cutoff of 1200 Ry. The atomic positions are relaxed so that the force on each atom is less than 0.04 eV Å^{-1}. The relaxed structural parameters are given in table 1. We sample the Brillouin zone on a uniform $32 \times 32 \times 32$ k-point mesh.

Figure 1 compares the electron density in $Ba_{0.6}K_{0.4}Fe_2As_2$ in GGA and GGA + A. From panel b of the figure it is clear that including the +A term transfers some of the electronic density from the iron atom to the outer region. The maximal relative change in the electronic density is about 7 % and it occurs on a charge density peak near the iron atom.

Figure 2 compares the band structure and the Fermi surface in GGA and GGA + A. We compare these results to the experiment in section 3.1.

In the GGA case, as in a previous calculation, [9] there are three hole pockets at the zone center (Γ), and two electron pockets at the zone corner (M). However, the band structures and the Fermi surfaces in GGA + A are both quantitatively and qualitatively different in several respects. First, the occupied bandwidth of the M-point d_{yz} and d_{zx} electron pockets in GGA + A is 4 meV (figure 2(a)), while it is 130 meV in GGA. In addition, the effective mass of these pockets is increased by a factor of 3–4 in GGA + A and the shape of the Fermi pocket in GGA + A is more elongated towards the Γ and Z points.

Second, the area of the hole pockets at Γ and Z is changed in GGA + A. Specifically, in GGA + A the size of the d_{xy} hole pockets at Γ and Z is increased by a factor of 4, so that it is larger than remaining two pockets. In addition, the d_{z^2} hole pocket is not present at Z in GGA + A so that now there are only two hole pockets at the Z point (versus three hole pockets at Z in GGA). Therefore, a three-dimensional ellipsoidal Fermi surface exists at Γ in GGA + A.

3.1. Comparison with ARPES

Now we compare modifications in the band structure due to +A term with the currently available experimental data on $Ba_{0.6}K_{0.4}Fe_2As_2$ band structure.

First, in the angle-resolved photoemission spectroscopy (ARPES) experiment, three hole pockets are observed at the zone center and the largest pocket is shown to originate from d_{xy} orbital [28] as in our GGA + A calculation. Second, large elongation of the M point pocket towards the Γ and Z points, we find using +A was experimentally observed in angle-resolved photoemission spectroscopy from [34]. Third, the presence of three-dimensional FS in $Ba_{0.6}K_{0.4}Fe_2As_2$ was suggested from c-axis polarized optical measurements [35]. The optical experiment found that the c-axis data only exhibit a small difference across T_c. This indicates the existence of three-dimensional FS with a dispersive band along the c axis.

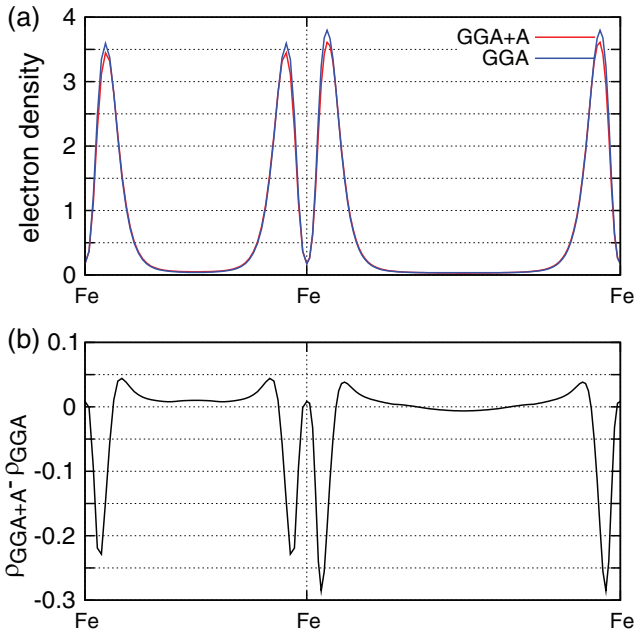

Figure 1. (a) The electron density of $Ba_{0.6}K_{0.4}Fe_2As_2$ in the nonmagnetic state on a line between the nearest-neighbor (left) and next-nearest-neighbor (right) iron atoms within GGA (blue) and GGA + A (red). Difference between GGA and GGA + A is shown in panel (b). Densities of both semi-core (3s, 3p) and valence (3d, 4s) states are included in our pseudopotential calculation.

4. Specific heat

In this section we discuss the calculated specific heat of $Ba_{0.6}K_{0.4}Fe_2As_2$. The specific heat coefficient γ_n is defined as,

$$\gamma_n = (1 + \lambda)\gamma_0. \quad (4)$$

Here γ_0 is the Sommerfeld coefficient proportional to DOS at the Fermi energy, and λ is the electron–phonon coupling coefficient.

First we discuss the density of states in GGA and GGA + A. In GGA the DOS at the Fermi energy of nonmagnetic $Ba_{0.6}K_{0.4}Fe_2As_2$ is 4.4 states eV^{-1} f.u.$^{-1}$ (the energy dependence of DOS is shown in figure 3). Similar value (3.1–5.5 states eV^{-1} f.u.$^{-1}$) for DOS was found in previous calculations [9, 10].

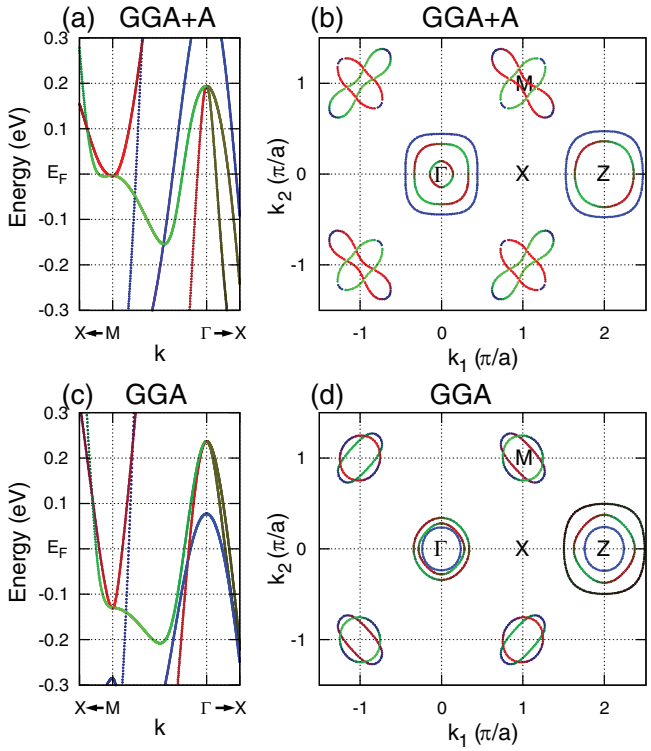

Figure 2. Electronic band structures and Fermi surface of $Ba_{0.6}K_{0.4}Fe_2As_2$ in the nonmagnetic states both in GGA + A (panels (a) and (b)) and in GGA (c, d). Dominant orbital characters (defined in the single-iron unit cell) are represented in blue (d_{xy}), red (d_{yz}), green (d_{zx}), black (d_{z^2}), and yellow (both d_{yz} and d_{zx}) color. High symmetry points in the Brillouin zone are defined in the two-iron unit cell. Reciprocal space axes k_1 and k_2 are perpendicular to the tetragonal c-axis.

In our GGA + A calculation, DOS at the peak value near the Fermi level is 11.9 states eV^{-1} $f.u.^{-1}$, almost three times larger than in GGA. Since γ_0 is proportional to DOS, it is also increased by a factor of 3 in GGA + A over GGA (see table 2).

Increase in the DOS after inclusion of +A term originates from the changes of the band structure at the M point. In the GGA + A, the bottom of the electron-like band at the M point (and the corresponding van Hove singularity) is placed almost at the E_F. Furthermore, the DOS at the van Hove singularity is enhanced due to the renormalization of the band width and the formation of a saddle point at the M point (figure 2(a)).

After having discussed the γ_0, we now discuss the contribution of the electron–phonon coupling coefficient (λ) to the heat capacity γ_n. We calculated the electron–phonon coupling coefficient λ using the Wannier interpolation technique [37] and the Quantum-ESPRESSO package [38].[1] The electron–phonon coupling in the nonmagnetic GGA + A calculation is 0.37, about two times larger than 0.18 obtained in GGA (see table 2). However, the heat capacity (γ_n) is proportional to $1 + \lambda$ so the increase in λ in GGA + A increases γ_n by 16 %, in addition to the dominant increase from larger DOS.

[1] We used an $8 \times 8 \times 8$ coarse k-mesh and a $4 \times 4 \times 4$ coarse q-mesh. The kinetic energy cutoff is 180 Ry and the smearing value is 2 mRyd. As in the case of calculations done with SIESTA, a full structural relaxation is performed with Quantum-ESPRESSO and the potassium doping is treated within the virtual crystal approximation.

Taking both terms together (γ_0 and $1 + \lambda$) we find that within GGA + A method specific heat coefficient γ_n equals 38 mJ mol^{-1} K^{-2}, which is much closer to the experimentally measured values (40–50 mJ mol^{-1} K^{-2}) than the GGA result (12 mJ mol^{-1} K^{-2}).

4.1. Antiferromagnetic ground states

So far we discussed the specific heat in the nonmangetic ground state of $Ba_{0.6}K_{0.4}Fe_2As_2$, now we consider two antiferromagnetic ground states: striped and checkerboard. The striped case is especially important, since this is the experimentally determined ground state of the parent compound $BaFe_2As_2$. We study the alternative ground state (checkerboard) for a comparison with the striped phase.

The (single-)stripe order consists of ferromagnetically arranged chains of iron atoms, with antiferromagnetic aligment between neighboring chains. On the other hand, in the checkerboard antiferromagnetic order magnetic moments on all neighboring iron atoms in point in opposite directions.

For easier comparison with the nonmagnetic calculations, in our magnetic GGA + A calculations we use the same value of A_c and the same function $f(r)$.

In the striped state, the peak in DOS occuring 50 meV below the Fermi level in GGA is shifted to 230 meV below the Fermi level when +A is included. However, there is no significant change in the value of DOS at the E_F (figures 3(c) and (f)). However, in the checkerboard state within GGA + A we obtain the DOS at E_F equal to 1.7 states eV^{-1} $f.u.^{-1}$, which is about one sixth of the GGA result (see figures 3(b) and (e)). This suppression in the checkerboard state is due to the occurrence of a Jahn–Teller distortion in GGA + A, which is lowering the crystal symmetry from tetragonal to orthorhombic.

Eventhough within GGA + A DOS at E_F is relatively small in the striped state (2.8 states eV^{-1} $f.u.^{-1}$) the electron–phonon coupling is significantly larger than in the nonmagnetic case. We obtained $\lambda = 0.90$ (see table 2) in striped state which is ∼60 % larger than in GGA. As we said earlier, DOS in striped state is nearly the same in GGA and GGA + A. Therefore, strong enhancement of λ in GGA + A must originate from other sources, and not simply from increased DOS. However, the origin of this enhancement is not the focus of this paper, and it will be reported elsewhere.

5. Conclusion

Increasing the potential on iron atoms (making them slightly more repulsive for electrons) improves the relevant structural (such as arsenic height and iron-arsenic-iron angle), magnetic, and electronic properties of $Ba_{0.6}K_{0.4}Fe_2As_2$, as calculated within DFT. The main result of this paper is that with a corrected potential (+A) on iron atom, the heat capacity of $Ba_{0.6}K_{0.4}Fe_2As_2$ is increased more than threefold, in good agreement with experimental data. Applying the same correction to the magnetic states, we find that electron–phonon coupling is strongly enhanced. This observation might be crucial

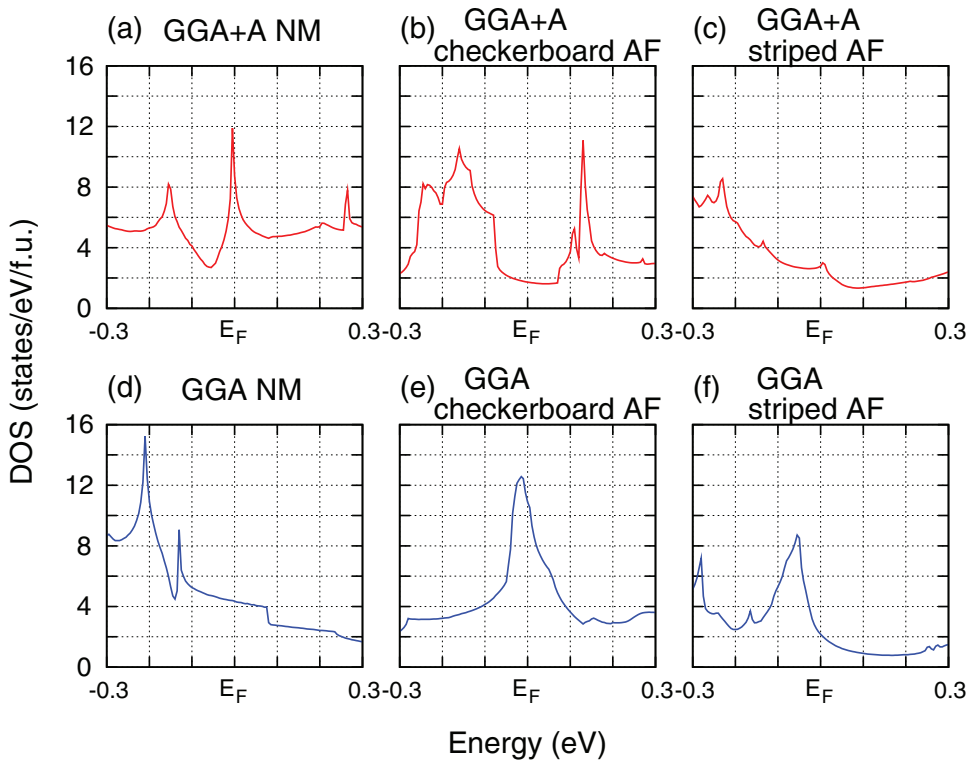

Figure 3. $Ba_{0.6}K_{0.4}Fe_2As_2$ density of states for both spin components, per two-iron formula unit in the nonmagnetic (NM), checkerboard antiferromagnetic, and single-stripe antiferromagnetic state, both in GGA + A (a)–(c) and GGA (d)–(f).

Table 2. A comparison of the Sommerfeld coefficient (γ_0), electron–phonon coupling (λ), and enhanced normal-state specific heat coefficient (γ_n) of $Ba_{0.6}K_{0.4}Fe_2As_2$ in GGA, GGA + A, and from experiment ([12–15]). Coefficients γ_0 and γ_n are given in mJ mol^{-1} K^{-2} in a two-iron atom unit cell and for both spin components.

	γ_0	λ	γ_n
Nonmagnetic			
GGA + A	28	0.37	38
GGA	10	0.18 [36]	12
Experiment			40–50
Checkerboard			
GGA + A	4.1	0.80	7.3
GGA	26	0.33 [36]	34
Single-stripe			
GGA + A	6.6	0.90	12
GGA	5.1	0.18 [36]	6.0

in understanding the superconducting properties of iron-based superconductors.

Acknowledgments

We thank Profs N E Phillips and R J Birgeneau for useful discussions. This work was supported by National Science Foundation Grant No. DMR10-1006184 (electronic and magnetic structure calculation) and by the Director, Office of Science, Office of Basic Energy Sciences, Materials Sciences and Engineering Division, US Department of Energy under Contract No. DE-AC02-05CH11231 (electron–phonon calculation). Computational resources have been provided by the DOE at Lawrence Berkeley National Laboratory's NERSC facility.

References

[1] Kamihara Y, Watanabe T, Hirano M and Hosono H 2008 *J. Am. Chem. Soc.* **130** 3296
[2] Stewart G 2011 *Rev. Mod. Phys.* **83** 1589
[3] Oh H, Moon J, Shin D, Moon C-Y and Choi H J 2011 *Prog. Supercond.* **13** 65 (arXiv: 1201.0237)
[4] Andersen O K and Boeri L 2011 *Ann. Phys.* **523** 8
[5] Dai P, Hu J and Dagotto E 2012 *Nat. Phys.* **8** 709
[6] Lu D H *et al* 2008 *Nature* **455** 81
[7] de la Cruz C *et al* 2008 *Nature* **453** 899
[8] Gretarsson H *et al* 2011 *Phys. Rev.* B **84** 100509
[9] Singh D J 2008 *Phys. Rev.* B **78** 094511
[10] Shein I R and Ivanovskii A L 2008 *JETP Lett.* **88** 107
[11] Hashimoto K *et al* 2010 *Phys. Rev.* B **82** 014526
[12] Popovich P, Boris A V, Dolgov O V, Golubov A A, Sun D L, Lin C T, Kremer R K and Keimer B 2010 *Phys. Rev. Lett.* **105** 027003
[13] Kant Ch, Deisenhofer J, Günther A, Schrettle F, Loidl A, Rotter M and Johrendt D 2010 *Phys. Rev.* B **81** 014529
[14] Storey J G, Loram J W, Cooper J R, Bukowski Z and Karpinski J 2013 *Phys. Rev.* B **88** 144502
[15] Rotundu C R, Forrest T R, Phillips N E and Birgeneau R J 2014 (arXiv: 1411.0116v2)
[16] Kim J S, Faeth B D and Stewart G R 2012 *Phys. Rev.* B **86** 054509
[17] Yin Z P, Haule K and Kotliar G 2011 *Nat. Mater.* **10** 932
[18] Tomczak J M, van Schilfgaarde M and Kotliar G 2012 *Phys. Rev. Lett.* **109** 237010
[19] Hansmann P, Arita R, Toschi A, Sakai S, Sangiovanni G and Held K 2010 *Phys. Rev. Lett.* **104** 197002

[20] Wang G-T, Qian Y, Xu G, Dai X and Fang Z 2010 *Phys. Rev. Lett.* **104** 047002
[21] Rotter M, Tegel M and Johrendt D 2008 *Phys. Rev. Lett.* **101** 107006
[22] Coh S, Cohen M L and Louie S G 2015 *New J. Phys.* **17** 073027
[23] Cohen M L and Heine V 1970 *Solid State Phys.* **24** 37
[24] Wang L-W and Zunger A 1995 *Phys. Rev.* B **51** 17398
[25] Perdew J P, Burke K and Ernzerhof M 1996 *Phys. Rev. Lett.* **77** 3865
[26] Sánchez-Portal D, Ordejón P, Artacho E and Soler J M 1997 *Int. J. Quantum Chem.* **65** 453
[27] Dederichs P H, Blügel S, Zeller R and Akai H 1984 *Phys. Rev. Lett.* **53** 2512
[28] Evtushinsky D V *et al* 2014 *Phys. Rev.* B **89** 064514
[29] Neupane M *et al* 2011 *Phys. Rev.* B **83** 094522
[30] Zhao J *et al* 2008 *Nat. Mater.* **7** 953
[31] Lee C-H, Iyo A, Eisaki H, Kito H, Fernandez-Diaz M T, Ito T, Kihou K, Matsuhata H, Braden M and Yamada K 2008 *J. Phys. Soc. Japan* **77** 083704
[32] Kuroki K, Usui H, Onari S, Arita R and Aoki H 2009 *Phys. Rev.* B **79** 224511
[33] Mizuguchi Y, Hara Y, Deguchi K, Tsuda S, Yamaguchi T, Takeda K, Kotegawa H, Tou H and Takano Y 2010 *Supercond. Sci. Technol.* **23** 054013
[34] Malaeb W *et al* 2012 *Phys. Rev.* B **86** 165117
[35] Cheng B *et al* 2011 *Phys. Rev.* B **83** 144522
[36] Boeri L, Calandra M, Mazin I I, Dolgov O V and Mauri F 2010 *Phys. Rev.* B **82** 020506
[37] Giustino F, Cohen M L and Louie S G 2007 *Phys. Rev.* B **76** 165108
[38] Giannozzi P *et al* 2009 *J. Phys.: Condens. Matter* **21** 395502